OPEN ACCESS
IOP Publishing
Journal of Optics
J. Opt. **16** (2014) 105712 (10pp)
doi:10.1088/2040-8978/16/10/105712

Scattering and absorption of a complex source point beam by a grounded lossy dielectric slab with a superstrate

Nikolaos L Tsitsas[1], **Constantinos A Valagiannopoulos**[2] **and Alexander I Nosich**[3]

[1] Department of Informatics, Aristotle University of Thessaloniki, Thessaloniki 54124, Greece
[2] Department of Radio Science and Engineering, School of Electrical Engineering, Aalto University, Espoo 02150, Finland
[3] Laboratory of Micro and Nano Optics, Institute of Radio-Physics and Electronics NASU, Kharkiv 61085, Ukraine

E-mail: ntsitsas@csd.auth.gr

Received 20 May 2014, revised 14 July 2014
Accepted for publication 18 July 2014
Published 26 September 2014

Abstract

Considered is the scattering and absorption of an E-polarized two-dimensional (2D) beam generated by a complex-source-point (CSP) feed in the presence of a lossy grounded dielectric slab with a lossless superstrate. The solution is found analytically in the Fourier-transform domain. Numerical results demonstrate the ways of obtaining enhanced absorption in the slab by a proper selection of the slab electrical thickness and the parameters of the superstrate. The effects of internal resonances in the slab are analyzed and discussed.

Keywords: absorption, complex source point (CSP) beam, Fourier integrals, scattering, slab structure

(Some figures may appear in colour only in the online journal)

1. Introduction

A large number of microwave and optical-wave applications depend on the efficiency of the absorption of the power radiated by an aperture source (such as small horn) in a flat layer of lossy material. Among them are hyperthermia, microwave drying, and solar-cell absorbers to mention only a few. Regarding these applications, one must typically choose the optimal parameters of the layer, the working wavelength, and the source placement. Preliminary analytical and numerical simulation of the corresponding wave scattering and absorption problem can lead to more efficient and cheaper technologies. Earlier works in this area have considered plane-wave illumination of a dielectric layer [1–6], which fails to take into account the finite size of illuminated spots in a real situation.

In contrast, our paper is aimed at considering a directive source placed at a finite distance from the lossy layer; this consideration corresponds more closely to an actual experimental situation. As our source, we use a complex-source-point (CSP) beam proposed in the early 1970s [7, 8] as a simplified model of a horn-like emitter radiating a unidirectional beam with controlled directivity. Note that in the 1980s–1990s the CSP beams were used by L. Felsen and E. Jull with co-authors, in combination with high-frequency asymptotic techniques [9–12], and in the 1990s by other authors together with numerical methods [13–15]. In these works the CSP beam plays the role of directive incident field, which is an exact solution of the Helmholtz equation and satisfies the radiation condition at infinity, unlike the more conventional Gaussian beam field. More recently CSP beams have also been studied as a preferable expansion basis in the

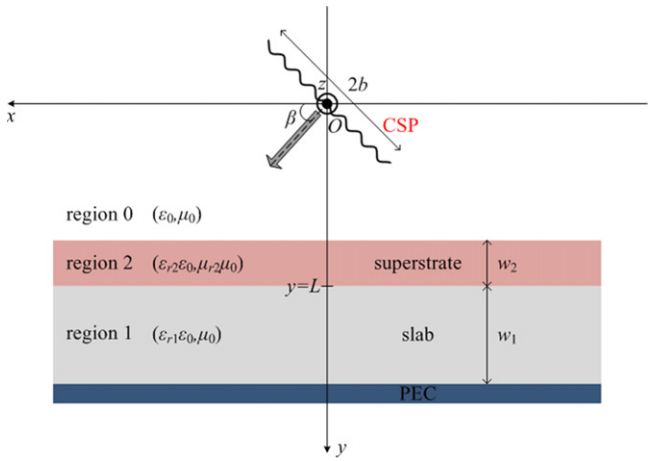

Figure 1. Cross-sectional geometry of the 2D structure under investigation composed of a planar dielectric slab lying between a PEC plane and a superstrate. The structure is excited externally by a CSP beam. The curvy line denotes the branch cut in real space, associated with CSP.

wave scattering problems [16, 17] dealing with large-size reflectors and lenses.

In section 2, we present the formulation of the problem and its solution in the Fourier-transform domain. Section 3 deals with the radiation and absorption characteristics. In section 4, numerical results are presented and resonance effects are discussed. The conclusions are summarized in section 5.

An exp($i\omega t$) time dependence is assumed and suppressed throughout, where ω is the angular frequency.

2. Mathematical modeling

2.1. Scattering geometry and primary field

Consider the two-dimensional (2D) configuration of figure 1, which is comprised of a perfect electric conducting (PEC) ground-plane and a lossy slab (region #1) of thickness w_1 and relative complex dielectric permittivity ε_{r1} covered by a lossless superstrate slab layer (region #2) of thickness w_2, relative real dielectric permittivity ε_{r2} and magnetic permeability μ_{r2}. The free half-space (vacuum region #0) above the superstrate is characterized by permittivity ε_0 and permeability μ_0. The entire structure is assumed uniform along the z-axis.

The above-described configuration is illuminated by a CSP beam generated by a primary electric current source with normalized current density

$$\mathbf{J}^{\mathrm{pr}}(x, y) = i\left(k_0 Z_0\right)^{-1}\delta(x - x_{CS})\delta(y - y_{CS})\hat{\mathbf{z}}, \qquad (1)$$

where δ denotes the delta function, $k_0 = \omega/c$ is the free-space wavenumber (with c for the light velocity), $Z_0 = \sqrt{\mu_0/\varepsilon_0}$ is the free-space impedance, and x_{cs} and y_{cs} are the complex coordinates of the source point given as

$$\begin{aligned}\mathbf{r}_{CS} = &\ (x_{CS}, y_{CS}) = \mathbf{r}_0 + i\mathbf{b}, \quad \mathbf{r}_0 = (x_0, y_0),\\ \mathbf{b} = &\ (-b\cos\beta, -b\sin\beta).\end{aligned} \qquad (2)$$

The real coordinates of the source are given by the vector $\mathbf{r}_0$, and we may consider, without loss of generality, that $(x_0, y_0) = (0, 0)$. The imaginary coordinates are given by the vector $\mathbf{b}$, and hence by the real parameters b and β, which are, respectively, associated with the aperture width and the orientation angle of a horn antenna simulated by a CSP [10–15]. The distance between the center (0,0) of the CSP and the upper boundary of the slab is denoted by L.

The z-component of the primary electric field radiated by the current source (1) is given by the Hankel function,

$$E^{\mathrm{pr}}(\mathbf{r}, \mathbf{r}_{CS}) = -\frac{i}{4}H_0^{(2)}\left(k_0\left|\mathbf{r} - \mathbf{r}_{CS}\right|\right). \qquad (3)$$

Note that if $b \neq 0$ then (3) has two singular points at $(x_0 \pm b\sin\beta, y_0 \mp b\cos\beta)$. This function is an exact solution of the Helmholtz equation with respect to the observation point $\mathbf{r}$,

$$\left(\Delta_{\mathbf{r}} + k_0^2\right)E^{\mathrm{pr}}(\mathbf{r}; \mathbf{r}_{CS}) = -\delta(\mathbf{r} - \mathbf{r}_{CS}), \qquad (4)$$

satisfying the Sommerfeld condition of radiation in 2D space. Moreover, it has a variable beam width controlled by the parameter $k_0 b$ as certified by the appearance of the exponential factor in the CSP far-field pattern [7–15],

$$\begin{aligned}&E^{\mathrm{pr}}(\mathbf{r}, \mathbf{r}_{CS}) \sim \sqrt{\frac{2}{\pi k_0 r}}\, e^{-i\left(k_0 r - \frac{\pi}{4}\right)}S^{\mathrm{pr}}(\varphi), \quad r \to \infty,\\ &S^{\mathrm{pr}}(\varphi) = -(i/4)e^{k_0 b\cos(\varphi+\beta)}, \quad 0 \leqslant \varphi \leqslant 2\pi,\end{aligned} \qquad (5)$$

where the polar coordinates are $r = \sqrt{x^2 + y^2}$, $\tan\varphi = y/x$.

2.2. Formulation of the scattering problem

In the presence of a slab, the total field is a sum of the CSP field (3) and the secondary field $E^{\mathrm{sec}}(\mathbf{r})$. The latter function must satisfy the homogeneous Helmholtz equation with the wavenumbers k_0 and $k_0\sqrt{\varepsilon_{r1,2}}$ in the free half-space, slab and superstrate, respectively, and, together with its normal derivative, the continuity conditions at the material interfaces. For uniqueness, it must also obey a certain radiation condition. Generally speaking, in view of the infinite boundaries this condition has to be modified with respect to the free-space radiation condition because of possible presence of the guided waves [18]. However, as shown in [18], non-attenuating guided waves do not exist in the presence of losses in the slab or in the superstrate. Therefore, for a lossy slab we require that $E^{\mathrm{sec}}(\mathbf{r}) \to 0$ if $|x| \to \infty$ and $L - w_2 < y < L + w_1$ and impose Sommerfeld radiation condition at $y < L - w_2$,

$$\begin{aligned}&E^{\mathrm{sec}}(\mathbf{r}) \sim \sqrt{\frac{2}{\pi k_0 r}}\, e^{-i\left(k_0 r - \frac{\pi}{4}\right)}S^{\mathrm{sec}}(\varphi), \quad r \to \infty,\\ &\pi \leqslant \varphi \leqslant 2\pi\end{aligned} \qquad (6)$$

2.3. Solution in the Fourier transform domain

In order to analytically solve the scattering problem with infinite along the x-axis boundaries, we express the primary field as a Fourier integral,

$$E^{\mathrm{pr}}(x, y; x_{CS}, y_{CS}) = \frac{1}{4\pi}\int_{-\infty}^{+\infty} g_0^{-1} e^{-i\lambda(x-x_{CS})} e^{\mp g_0(y-y_{CS})} d\lambda, \quad |y| > b|\cos\beta|, \tag{7}$$

where $g_0(\lambda) = (\lambda^2 - k_0^2)^{1/2}$ with either $\mathrm{Re}\{g_0(\lambda)\}>0$ or $\mathrm{Im}\{g_0(\lambda)\}>0$, so that the integrand function $e^{\mp g_0(y-y_{CS})}$ satisfies either the 1D radiation condition at $|y| > b|\cos\beta|$ or decays exponentially, depending on the value of λ.

Note that the inequality $|y| > b|\cos\beta|$ provides convergence of the integrals in the two branches of (7), determined by the factors $e^{\lambda b\cos\beta} e^{\mp\sqrt{\lambda^2-k_0^2}\, y} \sim e^{\lambda b\cos\beta} e^{\mp|\lambda| y}$. This means that we must choose the source and the slab-superstrate parameters L and w_2 in such a way that $b|\cos\beta| < L - w_2$ so that the CSP branch-cut does not intersect or touch the superstrate (see figure 1). Such limitations always appear naturally in the scattering problems associated with CSP beams (for instance, see [13]).

Now, the secondary field in regions #0, #1 and #2 can be also expressed as a Fourier integral,

$$E^{\mathrm{sec}}(x, y; x_{CS}, y_{CS}) = \frac{1}{4\pi}\int_{-\infty}^{+\infty} e^{-i\lambda(x-x_{CS})} \times \gamma\big(\lambda, y; y_{CS}\big)\, d\lambda. \tag{8}$$

Here the spectral function $\gamma(\lambda, y)$ under determination satisfies the appropriate 1D Helmholtz equation in the domains #0, #1, and #2 and the radiation or exponential-decay condition in the domain #0 ($y < L - w_2$), so that, respectively,

$$\gamma(y, \lambda) = \begin{cases} A_1 \exp\big[g_0\big(y - L + w_2\big)\big], \\ A_2 \cosh\left[g_2\left(y - L + \dfrac{w_2}{2}\right)\right] \\ + A_3 \sinh\left[g_2\left(y - L + \dfrac{w_2}{2}\right)\right], \\ A_4 \cosh\left[g_1\left(y - L - \dfrac{w_1}{2}\right)\right] \\ + A_5 \sinh\left[g_1\left(y - L - \dfrac{w_1}{2}\right)\right], \end{cases} \tag{9}$$

with $g_1(\lambda) = (\lambda^2 - k_0^2\varepsilon_{r1})^{1/2}$ and $g_2(\lambda) = (\lambda^2 - k_0^2\varepsilon_{r2}\mu_{r2})^{1/2}$; the values of these square roots can be chosen arbitrarily as the field in domains 1 and 2 and are not subject to a radiation condition.

The unknown spectral coefficients $A_i(\lambda)$, $i = 1,...5$ are determined analytically by imposing the boundary conditions at the boundaries $y = L - w_2$ and $y = L$ and the PEC boundary condition at $y = L + w_1$. The explicit expressions of these coefficients are given in the appendix.

3. Far-field characteristics and power considerations

As we are going to estimate the efficiency of absorption of the CSP beam in the lossy layer, we need a reference value of power. As such quantity, we first calculate the power radiated by an isolated CSP in free-space. In view of the total power flux continuity, this value can be calculated as the electromagnetic far-field power exiting the circle of large radius $|\mathbf{r}| = R \to \infty$,

$$P^{\mathrm{pr}} = \frac{1}{2}\,\mathrm{Re}\oint_{|\mathbf{r}|=R\to\infty}\left[\mathbf{E}^{\mathrm{pr}}(\mathbf{r}) \times \big(\mathbf{H}^{\mathrm{pr}}(\mathbf{r})\big)^*\right]\cdot d\mathbf{l}, \tag{10}$$

where * denotes the complex conjugate. On using the far-field asymptotic expression (5) to calculate the terms in (10), we obtain, similarly to [11],

$$P^{\mathrm{pr}} = \big(16\pi k_0 Z_0\big)^{-1}\int_0^{2\pi} e^{2k_0 b\cos(\varphi-\beta)} d\varphi,$$

which, by using equation (9.6.16) of [19], reduces to

$$P^{\mathrm{pr}} = \big(8k_0 Z_0\big)^{-1} I_0\big(2k_0 b\big)\ , \tag{11}$$

where I_0 is the zero order modified Bessel function. Note that the power P^{pr} can also be obtained based on the Complex Poynting Theorem, i.e. via the integration over a domain S, which contains the CSP projection to the real space (r, φ),

$$P^{\mathrm{pr}} = -\frac{1}{2}\,\mathrm{Re}\int_S\left[\mathbf{E}^{\mathrm{pr}}(\mathbf{r}, \mathbf{r}_{CS}) \cdot \big(\mathbf{J}^{\mathrm{pr}}(\mathbf{r}, \mathbf{r}_{CS})\big)^*\right] dS. \tag{12}$$

The domain S can be shrunk to the branch cut associated with CSP and finally to two disks centered at the branch cut endpoints. Then the use of the addition theorem (see equation (3) of [13]) and the property of the delta-function yield the same result as (11).

Second, we calculate the total power radiated by the CSP in the presence of the layered slab. By means of (5), (7), and (8), the total radiated electric field is expressed, for $y < -b|\cos\beta|$, as

$$\begin{aligned} E_z^{\mathrm{rad}}(x, y; b, \beta) &= E_z^{\mathrm{pr}}(x, y; b, \beta) + E_z^{\mathrm{sec}}(x, y; b, \beta) \\ &= \frac{1}{4\pi}\int_{-\infty}^{+\infty} g_0^{-1} e^{-i\lambda(x+ib\cos\beta)} e^{g_0(\lambda)(y+ib\sin\beta)} \\ &\quad \times [1 + A(\lambda)]\, d\lambda, \end{aligned} \tag{13}$$

where

$$A(\lambda) = A_1(\lambda) g_0(\lambda) e^{g_0(\lambda)\left(-L+w_2-ib\sin\beta\right)}. \tag{14}$$

Further, we calculate the magnetic field components from the Maxwell equations. Then, we use the upper line in (9) for the computation of the power exiting the semi-circle of radius $R \to \infty$ in region #0. The evaluation of Fourier integrals is

performed using the stationary phase formula (see e.g. [19]),

$$\int_{-\infty}^{+\infty} S(\lambda)\, e^{R\left(-\sqrt{\lambda^2-k_0^2}\,\sin\varphi - i\lambda\cos\varphi\right)} \times d\lambda \sim -\pi k_0 \sin\varphi \sqrt{\frac{2}{\pi k_0 R}}\, e^{-i\left(k_0 R-\frac{\pi}{4}\right)} S\left(k_0\cos\varphi\right), \quad R\to+\infty, \tag{15}$$

which yields

$$P^{\mathrm{rad}} = \frac{1}{16\pi k_0 Z_0} \times \int_{\pi}^{2\pi} e^{2k_0 b\cos(\varphi-\beta)} \left|1 + A\left(k_0\cos\varphi\right)\right|^2 d\varphi. \tag{16}$$

Note that if the slab, the superstrate and the ground plane are absent then no scattering occurs and $A=0$. In that case (16) gives a corresponding part of the power P^{pr}.

We also need the electromagnetic power absorbed by the lossy slab. By definition, this power is

$$P^{\mathrm{abs}} = \frac{k_0}{2Z_0}\,\mathrm{Im}\,\varepsilon_{r1}\int_{L}^{L+w_1}\int_{-\infty}^{+\infty} |E^{sec}(x,\, y;\, b,\, \beta)|^2 dx\, dy \tag{17}$$

According to the Poynting Theorem, it can also be found as the power flux through the upper interface $y=L$ of the slab,

$$P^{\mathrm{abs}} = \frac{1}{2}\,\mathrm{Re}\int_{-\infty}^{+\infty} E_z^{\mathrm{sec}}(x,\, L;\, b,\, \beta) H_x^{\mathrm{sec}\,*}(x,\, L;\, b,\, \beta) dx. \tag{18}$$

Equation (18) is more attractive than equation (17) because it involves single integration only. By substituting the field expressions into (18), changing the orders of integration, and using the basic property definition of the delta function, we arrive at

$$P^{\mathrm{abs}} = -k_0\left(16\pi Z_0\right)^{-1}\mathrm{Im}\,\varepsilon_{r1}\int_{-\infty}^{+\infty} e^{2\lambda\, b\cos\beta}|B(\lambda)|^2 \times\left[\frac{\sinh\left(2\,\mathrm{Re}\left\{g_1(\lambda)\right\}w_1\right)}{\mathrm{Re}\left\{g_1(\lambda)\right\}} - \frac{\sin\left(2\,\mathrm{Im}\left\{g_1(\lambda)\right\}w_1\right)}{\mathrm{Im}\left\{g_1(\lambda)\right\}}\right] d\lambda, \tag{19}$$

where

$$B(\lambda) = e^{-g_0\left(L-w_2+ib\sin\beta\right)}\times\left\{\cosh\left(g_2 w_2\right)\left[g_1\cosh\left(g_1 w_1\right)+g_0\sinh\left(g_1 w_1\right)\right] + \sinh\left(g_2 w_2\right)\left[\frac{\mu_{r2}\, g_0 g_1}{g_2}\cosh\left(g_1 w_1\right)+\frac{g_2}{\mu_{r2}}\sinh\left(g_1 w_1\right)\right]\right\}^{-1}. \tag{20}$$

We have also checked that on substituting into (18) the Fourier integral (8) for $E^{\mathrm{sec}}(x,\, y)$, changing the order of integration in the space coordinates x and y and in the spectral parameter λ, and integrating in x and y analytically we obtain a single integral in λ that is identical with (19).

In order to estimate the effect of the lossless superstrate (region #2) on the total electromagnetic power absorbed in region #1, we introduce (in a similar way to [20]; see also [21]), the following *enhancement factor*

$$EF = P^{\mathrm{abs}}/\tilde{P}^{\mathrm{abs}}, \tag{21}$$

where the powers P^{abs} and $\tilde{P}^{\mathrm{abs}}$ correspond, respectively, to the cases with and without the superstrate. Beneficial influence of the superstrate layer, leading to an enhanced absorption (needed, for instance, for development of efficient solar cells), is demonstrated if $EF>1$.

It is also possible to see that EF can be equivalently understood as the ratio of the power stored in the slab when the superstrate is present over the same power when it is absent. This is because according to the Poynting Theorem these two powers relate as $P^{\mathrm{abs}}/P^{\mathrm{stored}} = -\mathrm{Im}\,\varepsilon_{r1}/\mathrm{Re}\,\varepsilon_{r1}$.

4. Numerical results and discussions

In computations, we have to integrate the expressions (16) and (19) numerically. When integrating in λ, it is convenient to cast the integrand to a dimensionless form after introduction of the normalized quantities

$$\tilde{\lambda} = \frac{\lambda}{k_0},\quad \tilde{g}_j\left(\tilde{\lambda}\right) = \sqrt{\tilde{\lambda}^2 - \frac{k_j^2}{k_0^2}}\ (j=0,1,2).$$

First of all, as a partial validation of the derived analytical results and computer code, we present in figure 2 the normalized powers $P^{\mathrm{abs}}/P^{\mathrm{pr}}$ and $P^{\mathrm{rad}}/P^{\mathrm{pr}}$ versus the angle β for (a) $k_0 w_1 = 1.5,\ 2,\ 2.5$ with $L=10w_1$ and (b) $L/w_1 = 2,\ 5$ with $k_0 w_1 = 2.36$.

From figure 2 we observe that if the CSP is placed far from a thin slab ($L=10w_1$ and $k_0 w_1 = 1.5$) and its beam 'looks away' from the slab ($\beta = 3\pi/2$) then $P^{\mathrm{rad}}/P^{\mathrm{pr}} \approx 1$ and $P^{\mathrm{abs}}/P^{\mathrm{pr}} \approx 0$. This is expected because in this situation the influence of the slab is a minimum and the field radiated by the CSP is very close to the complex beam in free space. Moreover, the largest values of $P^{\mathrm{abs}}/P^{\mathrm{pr}}$ are obtained for $\beta=\pi/2$, corresponding to the normal incidence on the slab. Besides, $P^{\mathrm{abs}}/P^{\mathrm{pr}}$ ($P^{\mathrm{rad}}/P^{\mathrm{pr}}$) increases (decreases) with larger $k_0 w_1$ and smaller L/w_1. These facts could be attributed to the different evanescent components of the electromagnetic field that reach the slab as the distance L is decreased.

Then we proceed to seek the resonance regimes in the scattering and absorption. To this end we need the dependences of the powers on the normalized frequency. We have selected that quantity as the electrical thickness of the slab, $k_0 w_1$. Other involved parameters are normalized by w_1 in order to have a fixed geometry but varying frequency. As a sensing tool to detect resonances of the slab as an open cavity, the best is the normalized absorbed power $P^{\mathrm{abs}}/P^{\mathrm{pr}}$ because the radiated power is associated with the far field, not with the field inside the cavity.

In figure 3, we present the powers $P^{\mathrm{abs}}/P^{\mathrm{pr}}$ and $P^{\mathrm{rad}}/P^{\mathrm{pr}}$ and the enhancement factor EF versus the electric thickness of the slab $k_0 w_1$ for $\varepsilon_{r2}=1,\ 2$, and 3 with $\varepsilon_{r1}=5(1-0.05i)$, $w_2 = w_1/10$, $b=w_1/3$, $\beta=\pi/2$, and $L=10w_1$. These plots display resonances caused by the corresponding complex-valued

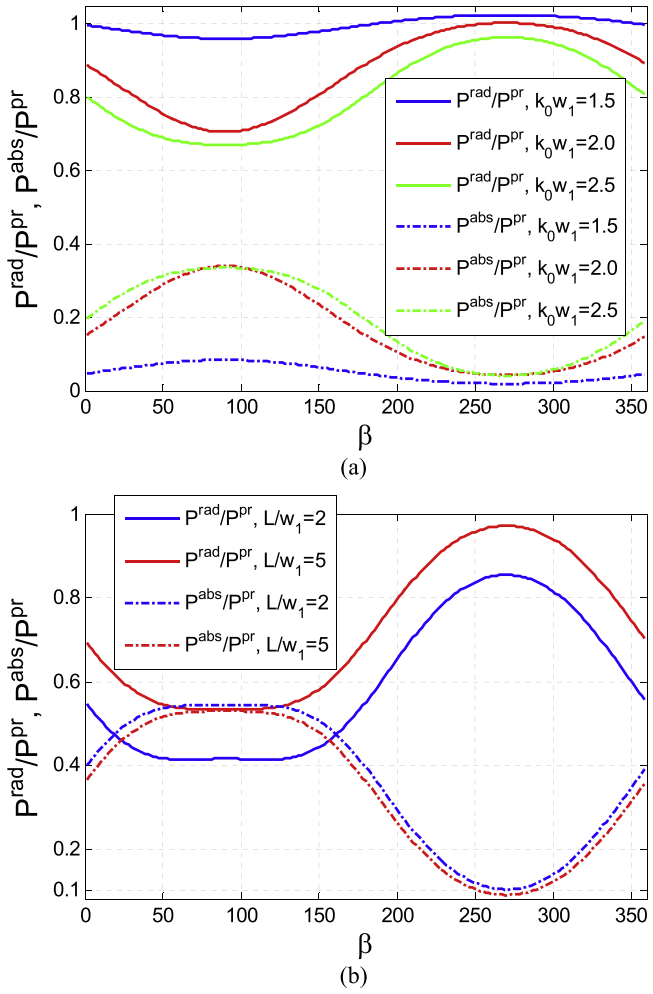

Figure 2. Normalized absorbed and radiated powers $P^{\rm abs}/P^{\rm pr}$ and $P^{\rm rad}/P^{\rm pr}$ as functions of the CSP beam orientation angle β for (a) $k_0w_1 = 1.5$, 2, 2.5 with $L = 10w_1$ and (b) $L/w_1 = 2$, 5 with $k_0w_1 = 2.36$ for (in both (a) and (b)) a bare slab ($\varepsilon_{r2} = \mu_{r2} = 1$) with $\varepsilon_{r1} = 5$ (1–0.05i), $b = w_1/3$.

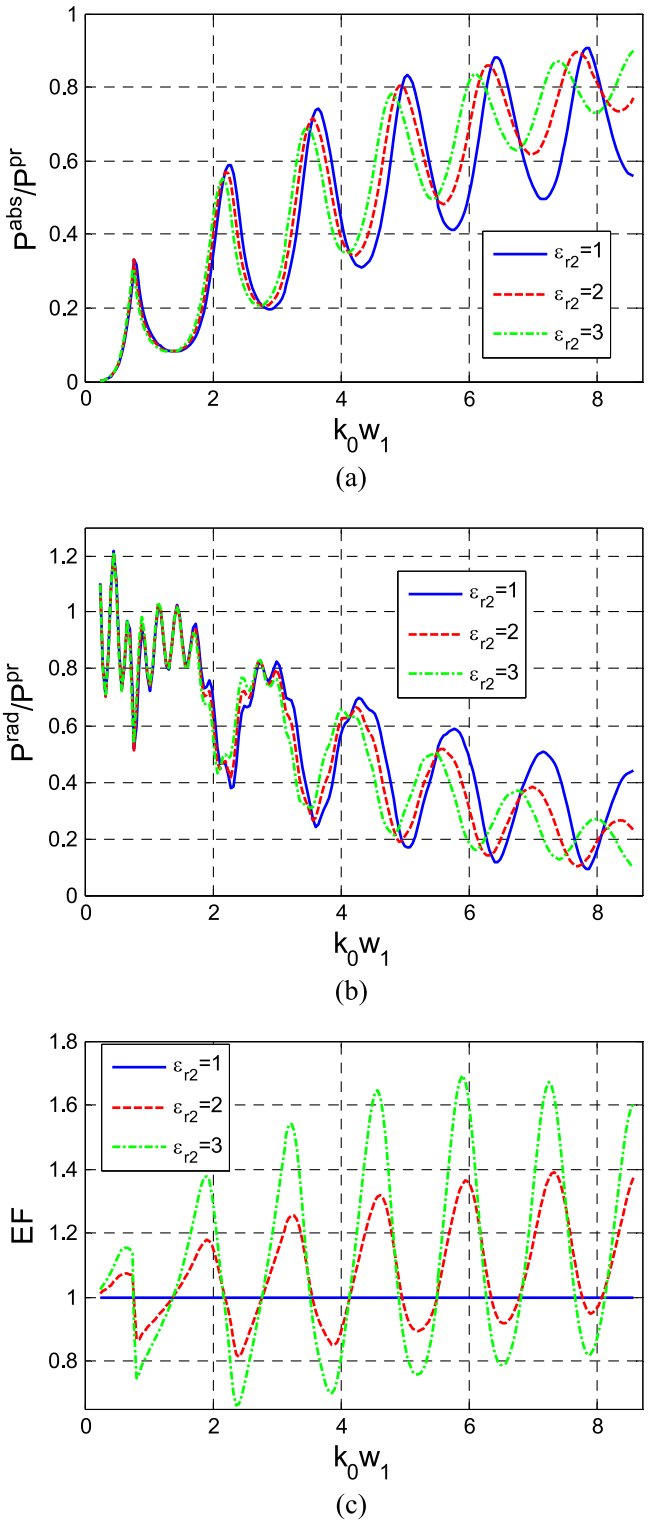

Figure 3. Normalized absorbed and radiated powers $P^{\rm abs}/P^{\rm pr}$ and $P^{\rm rad}/P^{\rm pr}$ and enhancement factor EF as functions of the electric thickness of the slab k_0w_1 for different values of the superstrate permittivity $\varepsilon_{r2} = 1$, 2, and 3 with $\varepsilon_{r1} = 5(1–0.05i)$, $w_2 = w_1/10$, $\mu_{r2} = 1$, $b = w_1/3$, $\beta = \pi/2$, and $L = 10w_1$. Note that $EF = 1$ when $\varepsilon_{r2} = 1$ because at that point the superstrate is absent.

poles of the field as a function of frequency. As known, if the Q-factor of a natural mode is not very small then the location of the maximum in $P^{\rm abs}$ is close to the real part of the pole.

The natural-mode frequencies of a single-layer dielectric slab backed by a PEC plane as a 1D open resonator satisfy the characteristic equation,

$$\cot\left(k_0 w\sqrt{\varepsilon_{r1}}\right) = 1/\varepsilon_{r1}. \tag{22}$$

If $|\varepsilon_{r1}| \gg 1$ then the roots of (22) have their asymptotic form as

$$k_0 w \approx (\pi/2)\, m\, \varepsilon_{r1}^{-1/2},\quad m = 1,\ 3,... \tag{23}$$

In our case Re$\{\varepsilon_{r1}\}$ is only 5, however there is still quite good agreement of (23) with the resonance frequencies of $P^{\rm abs}$.

In particular, the first resonance in $P^{\rm abs}$ in figure 3(a) appears at $k_0w_1 = 0.76$, while the value obtained from (23) is 0.7. We can also observe that for the covered slab case, if $\varepsilon_{r2} = 2$ and 3, the resonances gradually shift to the left. This can be explained by the widening of the considered cavity. At higher frequencies, the superstrate acts as a second cavity and brings its own natural modes (i.e. complex-valued poles). Then, the whole layered-slab structure behaves as a coupled cavity where all modes are hybrid (also known as

supermodes). These effects are not visible in figure 3 due to too-small electrical width of the superstrate ($k_0 w_2 \sqrt{\varepsilon_{r2}} < \pi/2$); they should appear at higher frequencies. Some of the above remarks may also be justified by means of the impedance matching effect of the superstrate. For example the first peak at $k_0 w_1 = 0.76$ can be seen as the first point where the input impedance seen at the top of the dielectric superstrate gets closest to a match.

Worth noting is that the peaks in P^{abs} (i.e. natural-mode resonances) do not coincide with peaks in *EF* in frequency. This means that a thin superstrate with a smaller than the slab permittivity works only off the resonance that can be attractive in applications where broadband absorption is needed.

In practical situations, we normally expect that the source is fixed and releases the same power at a fixed frequency, lost for the scattering and the absorption. Hence, we want the sum $P^{\text{rad}} + P^{\text{abs}}$ to depend weakly on the parameters of the slab and the superstrate. This requirement is generally achieved for the curves presented in figure 3: the value $(P^{\text{rad}} + P^{\text{abs}})/P^{\text{pr}}$ is close to 1 (however not equal to 1) and varies slightly if, at least, $k_0 w_1 \geqslant 2$. This is apparently because the CSP is quite far from the slab, in terms of the wavelength (here, $k_0 L \geqslant 20$). If, however, $k_0 w_1 < 2$ then the frequency scan of the radiated power, P^{rad}, shows many ripples (figure 3(b)), which are insensitive to the presence of the superstrate. The scan of P^{abs} remains smooth and has no ripples. Close inspection shows that the ripples are explained by the interference, in the far zone, of the primary CSP-beam field and the field of its image in the PEC ground plane covered with a dielectric slab. Indeed, if $k_0(L + w_1) \to 0$ then the power P^{rad} diverges because the Maxwell equations do not allow putting the electric source on the PEC plane, and this divergence is oscillatory.

Now, we will suppose that the slab, the source and the frequency are fixed, and the product $k_0 w_1$ is tuned to the first resonance of P^{abs}. Then, only the superstrate parameters w_2/w_1 and ε_{r2} remain to be varied in order to look for appropriately large *EF* values. This may need, according to the conclusions from figure 3, detuning from the original frequency to get to the shifted resonance position.

In general, for $\varepsilon_{r2} > \text{Re}\{\varepsilon_{r1}\}$ a larger *EF* could be expected because such a cavity with a denser thin superstrate will be 'less open' than a bare-slab cavity, implying that the *Q*-factors of the natural modes will get higher. On the other hand, a superstrate may spoil the coupling of the CSP beam field with a slab mode because of its larger reflection. Hence, there are two competing mechanisms and therefore a search for a larger *EF* may be not so straightforward.

In figure 4, we depict the powers $P^{\text{abs}}/P^{\text{pr}}$ and $P^{\text{rad}}/P^{\text{pr}}$ and the enhancement factor *EF* versus the dielectric permittivity ε_{r2} of the slab superstrate for the thickness values $w_2 = w_1/10$, $w_1/8$, and $w_1/6$. The frequency is fixed at $k_0 w_1 = 0.6$ which is taken to be on the left of the first resonance of the bare slab structure; the latter is $k_0 w_1 = 0.76$ according to figure 3(a). We observe that a thin superstrate that is electrically denser than the slab, e.g. with ε_{r2} from 8 to 14 depending on the ratio w_2/w_1, can yield $EF = 3$ but (as

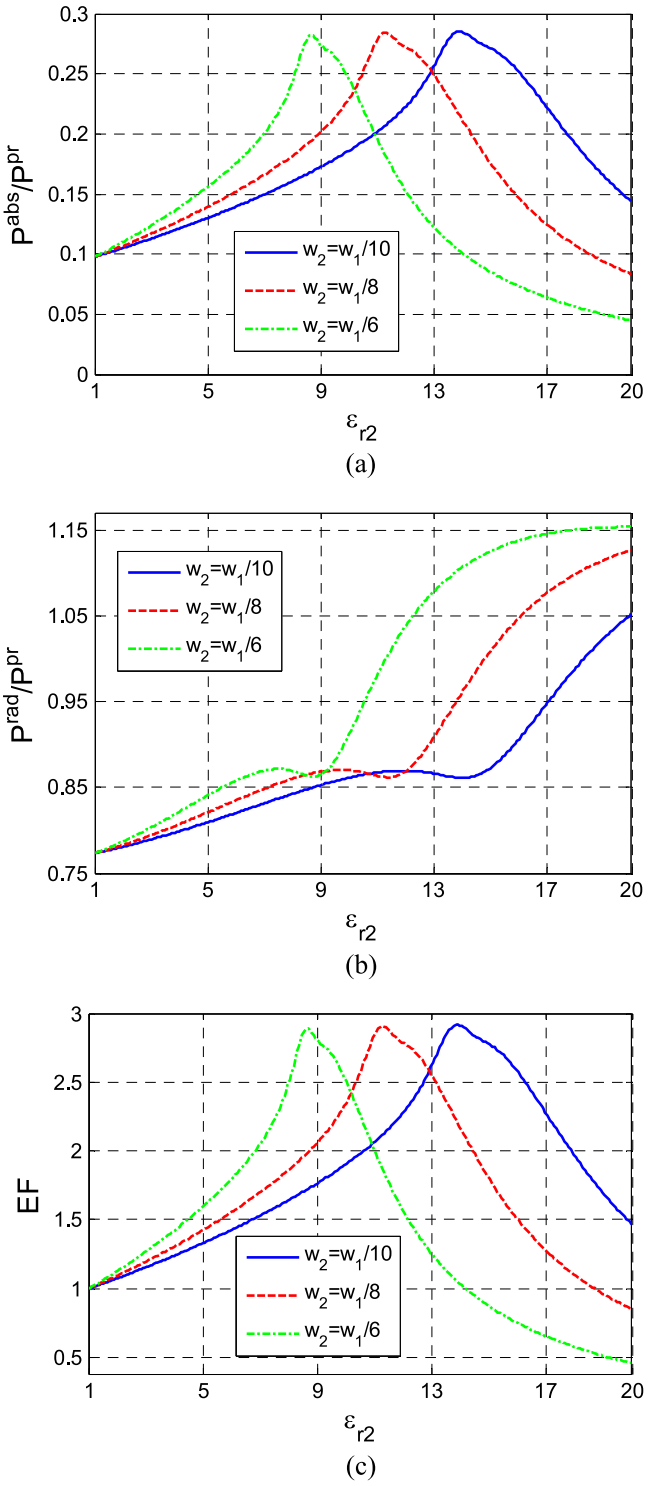

Figure 4. Normalized absorbed (a) and radiated (b) powers and enhancement factor (c) as functions of the dielectric permittivity ε_{r2} of the slab superstrate for different values of the superstrate thickness $w_2 = w_1/10$, $w_1/8$, and $w_1/6$ with $k_0 w_1 = 0.6$ and the other parameters being the same as in figure 3.

elaborated above) off the resonance peak of P^{abs}. The computed results have been presented in dimensionless units. A representative example in explicit dimensional units in the microwave region can be considered (according to the parameters of figure 4) by selecting a particular thickness of the

lossy slab $w_1 = 3$ mm and a free-space frequency of 9.54 GHz (resulting in electrical thickness $k_0 w_1 = 0.6$). The thickness of the lossless superstate is, then, $w_2 = 0.3$, 0.375, or 0.5 mm, the distance of the CSP from the slab is $L = 30$ mm, while the aperture width of the CSP is $b = 1$ mm.

Up to this point we have considered that $\mu_{r2} = 1$, i.e. that the superstrate is non-magnetic. Now, we investigate the effect of a magnetic superstrate with $\mu_{r2} > 1$ and $\varepsilon_{r2} = 1$. We suppose that the electrical width $k_0 w_1$ is tuned to the first resonance $k_0 w_1 = 0.76$ of P^{abs} of the bare slab; here we do not detune to a shifted resonance position. In figure 5, we show the powers $P^{\text{abs}}/P^{\text{pr}}$ and $P^{\text{rad}}/P^{\text{pr}}$ and the enhancement factor EF versus the magnetic permeability μ_{r2} of the slab superstrate for the same superstrate's thickness values considered in figure 4. We observe that a thin superstrate achieves increasing values of P^{abs} and EF and decreasing values of P^{rad} with increasing μ_{r2} on the resonance peak of P^{abs} of the bare slab. This shows that the permeability of the superstrate constitutes an additional control mechanism offering enhanced absorption and, importantly, without detuning from the original resonance frequency (as was the case in the variations with respect to ε_{r2} depicted in figure 4). The increase in P^{abs} can be attributed to the fact that by increasing μ_{r2} we are making the cavity less leaky through the upper boundary (the superstrate's refractive index and hence the contrast with respect to the bordering media are increased).

Furthermore, we have also computed frequency dependences (not included here) of the powers and the EF for the other values of the normalized aperture width b/w_1 and the orientation angle β of the CSP. The qualitative behavior of the respective quantities is similar to that depicted in figures 3 and 4, as long as the incident beam 'sees' the slab.

Regarding the distance L of the CSP from the slab, we note that if $L = 10w_1$, or larger, then the whole configuration serves as a model for horn antennas used for heating, drying, or pumping a lossy slab. If one has in mind other types of applications then smaller values of $k_0 L$ are also of interest. We have also performed simulations with smaller values of $k_0 L$ and found that the conclusions derived above concerning the variations of the powers still remain valid.

Next, we examine the variations of the absorbed and radiated powers in a high-frequency (HF) regime. Figure 6 depicts the normalized powers $P^{\text{abs}}/P^{\text{pr}}$ and $P^{\text{rad}}/P^{\text{pr}}$ versus the electric thickness of the slab $k_0 w_1$ for superstrate permittivity values $\varepsilon_{r2} = 1$, 2, 3 with $\varepsilon_{r1} = 5(1–0.05i)$, $w_2 = w_1/10$, $b = w_1/3$, $\beta = \pi/2$, and $L = 1.3w_1$. It is evident that there exist wide regions of the normalized frequency $k_0 w_1$ where $P^{\text{abs}}/P^{\text{pr}}$ is very close to 1 and simultaneously $P^{\text{rad}}/P^{\text{pr}}$ is very close to 0.

We examine this effect further and also test it with respect to the variations of the superstrate relative permittivity ε_{r2} by depicting in the panels of figure 7 the reliefs of $P^{\text{abs}}/P^{\text{pr}}$, $P^{\text{rad}}/P^{\text{pr}}$, $10\log_{10}(P^{\text{rad}}_{\text{with}}/P^{\text{rad}}_{\text{without}})$ and EF versus both $k_0 w_1$ and ε_{r2}. By 'with' and 'without' we mean that the structure is considered with and without the superstrate, respectively.

The region of $k_0 w_1$ from 27 to 37 and ε_{r2} from 1.8 to 2.8 is characterized by large absorption, where $P^{\text{abs}}/P^{\text{pr}}$ is very close to 1. This yields $EF > 1$ with a maximum value of $EF = 1.2$. Importantly, in the same region the radiated power

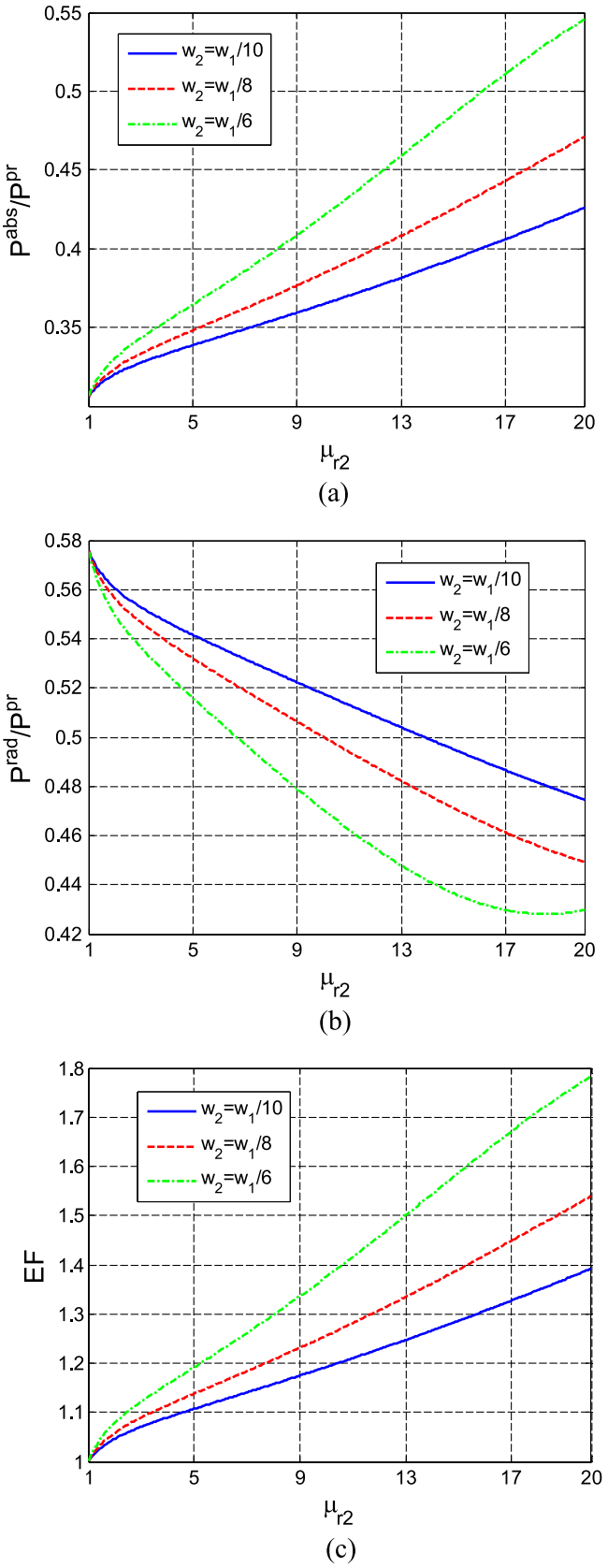

Figure 5. Normalized absorbed (a) and radiated (b) powers and enhancement factor (c) as functions of the magnetic permeability μ_{r2} of the slab superstrate for different values of the superstrate thickness with $\varepsilon_{r2} = 1$ and the other parameters being the same as in figure 4.

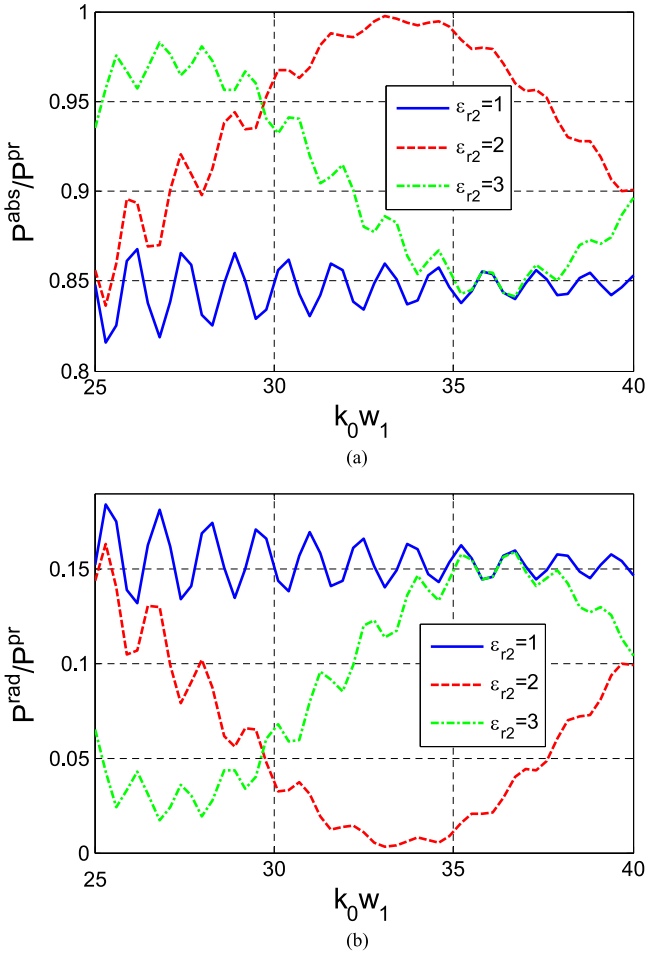

Figure 6. Normalized absorbed and radiated powers P^{abs}/P^{pr} and P^{rad}/P^{pr} as functions of the electric thickness of the slab k_0w_1 for different values of the superstrate's permittivity $\varepsilon_{r2}=1$, 2, and 3 with $\varepsilon_{r1}=5(1–0.05i)$, $w_2=w_1/10$, $\mu_{r2}=1$, $b=w_1/3$, $\beta=\pi/2$, and $L=1.3w_1$.

is decreased significantly with P^{rad}/P^{pr} being close to 0. This is emphasized by the variations of $10\log_{10}(P^{rad}_{with}/P^{rad}_{without})$ showing a 20 dB reduction in the radiated power for $(k_0w_1, \varepsilon_{r2})=(32, 2.2)$ compared to the no-superstrate case.

The above results can be considered as elementary optimization. More systematic optimization treatment can potentially provide even better results concerning combinations of parameters, which provide large absorption and reduced radiation.

5. Conclusions

We have considered the radiation and absorption of the directive CSP beam field in the presence of a lossy dielectric slab backed with a PEC plane. It has been shown that the radiated (absorbed) power has minima (maxima) associated with the excitation of the slab natural modes.

By covering the slab with a thin lossless superstrate one can enhance the power absorbed in the slab, although not at all frequencies. Larger enhancement can be achieved with electrically dense superstrates. To this end, the frequency and other parameters such as the superstrate thickness and its permittivity should be selected properly. This can be done by using the methodology and the equations presented in the paper.

Appendix

The coefficients appearing in the secondary fields expressions (7) and (8) are given by

$$A_1 = \frac{e^{-g_0(L-w_2-y_{CS})}}{g_0} \times \frac{K(g_0, g_1, g_2, w_2) - e^{-2g_1w_1}M(g_1, g_0, g_2, w_2)}{\Lambda(g_1, g_0, g_2, w_2) + e^{-2g_1w_1}K(g_1, g_0, g_2, w_2)} \quad (A.1)$$

$$A_2 = e^{-g_0(L-w_2-y_{CS})} \times \frac{P_o(g_1, g_2, w_2) - e^{-2g_1w_1}Q_o(g_1, g_2, w_2)}{\Lambda(g_1, g_0, g_2, w_2) + e^{-2g_1w_1}K(g_1, g_0, g_2, w_2)} \quad (A.2)$$

$$A_3 = -e^{-g_0(L-w_2-y_{CS})} \times \frac{P_e(g_1, g_2, w_2) + e^{-2g_1w_1}Q_e(g_1, g_2, w_2)}{\Lambda(g_1, g_0, g_2, w_2) + e^{-2g_1w_1}K(g_1, g_0, g_2, w_2)} \quad (A.3)$$

$$A_4 = e^{-g_0(L-w_2-y_{CS})}\frac{1}{\mu_{r2}}\frac{g_2}{2\cosh\left[g_1\frac{w_1}{2}\right]} \times \frac{1-e^{-2g_1w_1}}{\Lambda(g_1, g_0, g_2, w_2) + e^{-2g_1w_1}K(g_1, g_0, g_2, w_2)} \quad (A.4)$$

$$A_5 = -e^{-g_0(L-w_2-y_{CS})}\frac{1}{\mu_{r2}}\frac{g_2}{2\sinh\left[g_1\frac{w_1}{2}\right]} \times \frac{1-e^{-2g_1w_1}}{\Lambda(g_1, g_0, g_2, w_2) + e^{-2g_1w_1}K(g_1, g_0, g_2, w_2)} \quad (A.5)$$

In (A.1)–(A.5) are utilized the following auxiliary functions

$$P_e(f, g, d) = f\cosh\left(g\frac{d}{2}\right) + \frac{1}{\mu_{r2}}g\sinh\left(g\frac{d}{2}\right)$$

$$P_o(f, g, d) = \frac{1}{\mu_{r2}}g\cosh\left(g\frac{d}{2}\right) + f\sinh\left(g\frac{d}{2}\right)$$

$$Q_e(f, g, d) = f\cosh\left(g\frac{d}{2}\right) - \frac{1}{\mu_{r2}}g\sinh\left(g\frac{d}{2}\right)$$

$$Q_o(f, g, d) = \frac{1}{\mu_{r2}}g\cosh\left(g\frac{d}{2}\right) - f\sinh\left(g\frac{d}{2}\right)$$

$$\Lambda(e, f, g, d) = \frac{P_e(e, g, d)P_o(f, g, d) + P_o(e, g, d)P_e(f, g, d)}{2}$$

$$K(e, f, g, d) = \frac{Q_e(e, g, d)P_o(f, g, d) - Q_o(e, g, d)P_e(f, g, d)}{2}$$

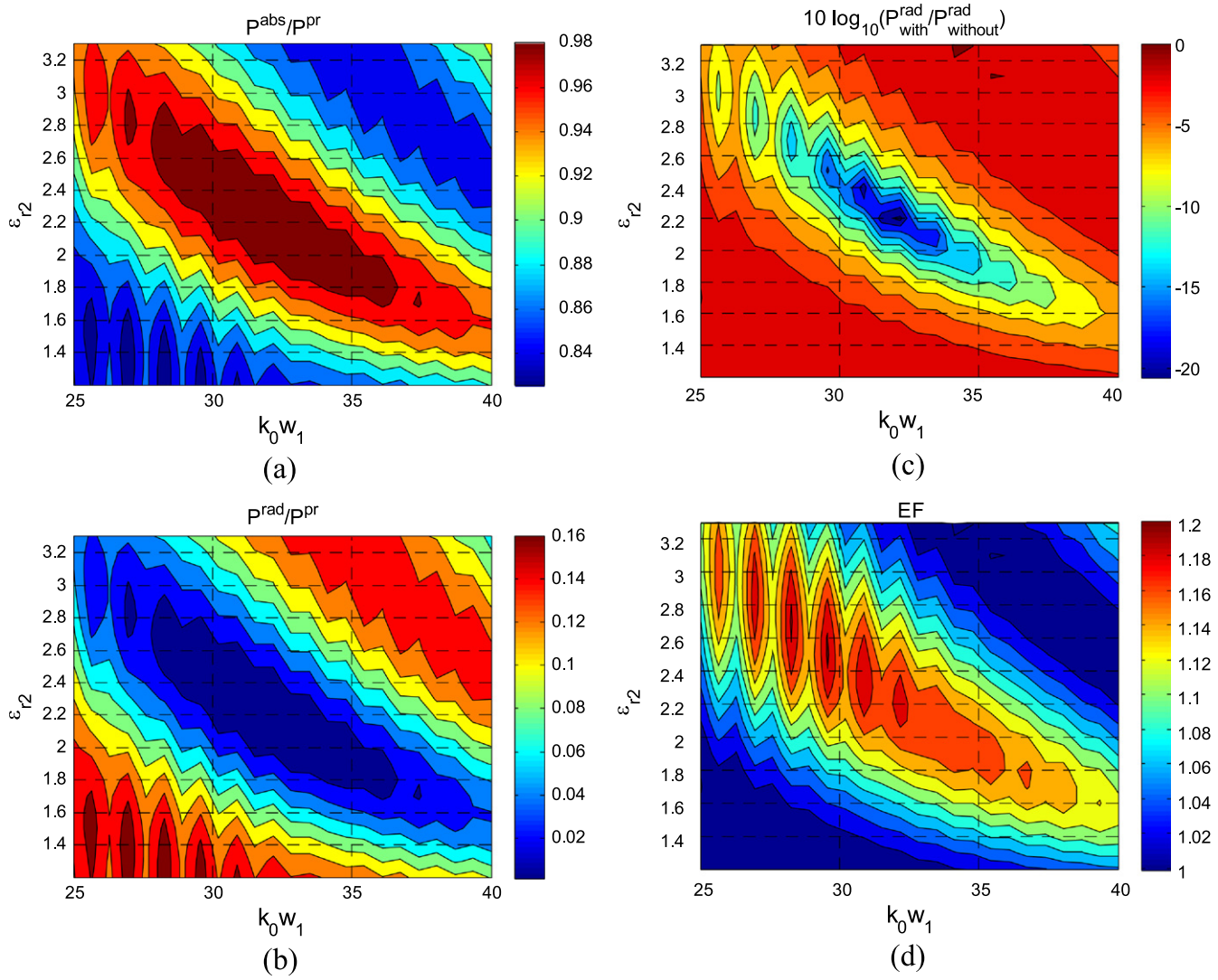

Figure 7. Contour plots of P^{abs}/P^{pr}, P^{rad}/P^{pr}, $10\log_{10}(P^{rad}_{with}/P^{rad}_{without})$, and *EF* versus the slab's electric thickness k_0w_1 and the superstrate's permittivity ε_{r2}. The remaining parameters are the same as in figure 6; 'with' and 'without' correspond to with and without superstrate.

$$M(e,f,g,d) = \frac{Q_o(e,g,d)Q_e(f,g,d) + Q_e(e,g,d)Q_o(f,g,d)}{2}$$

References

[1] Perini J and Cohen L S 1993 Design of broad-band radar absorbing material for large angle of incidence *IEEE Trans. Electromagn. Compat.* **35** 223–30

[2] Wenhua Y, Werner D H and Mittra R 2001 Reflection characteristic analysis of an artificially synthesized absorbing medium *IEEE Trans. Magnetics* **37** 3798–802

[3] Ratanadecho P, Aoki K and Akahori M 2002 A numerical and experimental investigation of the modeling of microwave heating for liquid layers using a rectangular wave guide (effects of natural convection and dielectric properties) *Appl. Math. Modelling* **26** 449–72

[4] Christ A, Samaras T, Klingenbock A and Kuster N 2006 Characterization of the electromagnetic near-field absorption in layered biological tissue in the frequency range from 30 MHz to 6000 MHz *Phys. Med. Biol.* **51** 4951–65

[5] Wang W, Wu S, Reinhardt K, Lu Y and Chen S 2010 Broadband light absorption enhancement in thin-film silicon solar cells *Nano Lett.* **10** 2012–8

[6] Micheli D, Pastore R, Apollo C, Marchetti M, Gradoni G, Primiani V M and Moglie F 2011 Broadband electromagnetic absorbers using carbon nanostructure-based composites *IEEE Trans. Microwave Theory Techn.* **59** 2633–46

[7] Deschamps G A 1971 The Gaussian beam as a bundle of complex rays *Electron. Lett.* **7** 84–5

[8] Izmestyev A A 1971 One-parametrical wave beams in free space *Izvestiya VUZ Radiofiz.* **13** 1380–6
Izmestyev A A 1971 *Radiophys. Quantum Electron.* **13** 1062–8

[9] Ra J W, Bertoni H L and Felsen L B 1973 Reflection and transmission of beams at a dielectric interface *SIAM J. Appl. Math.* **24** 396–413

[10] Felsen L B 1975 Complex source-point solutions of the field equations *Symp. Math.* **18** 39–56

[11] Jull E V and Suedan G A 1987 Beam diffraction by a half-plane and a wide slit *IEEE Trans. Antennas Propagat.* **35** 1077–83

[12] Suedan G A and Jull E V 1991 Beam diffraction by planar and parabolic reflectors *IEEE Trans. Antennas Propagat.* **39** 521–7
[13] Oguzer T, Altintas A and Nosich A I 1995 Accurate simulation of reflector antennas by the complex source-dual series approach *IEEE Trans. Antennas Propagat.* **43** 793–801
[14] Boriskina S V, Nosich A I and Altintas A 2000 Effect of the imperfect flat earth on the vertically-polarized radiation of a cylindrical reflector antenna *IEEE Trans. Antennas Propagat.* **48** 285–92
[15] Boriskin A V and Nosich A I 2002 Whispering-gallery and Luneburg-lens effects in a beam-fed circularly layered dielectric cylinder *IEEE Trans. Antennas Propagat.* **50** 1245–9
[16] Skokic S, Casaletti M, Maci S and Sørensen S B 2011 Complex conical beams for aperture field representations *IEEE Trans. Antennas Propagat.* **59** 611–22
[17] Tap K, Pathak P H and Burkholder R J 2011 Exact complex source point beam expansions for electromagnetic fields *IEEE Trans. Antennas Propagat.* **59** 3379–90
[18] Nosich A I 1994 Radiation conditions, limiting absorption principle, and general relations in open waveguide scattering *J. Electromagn. Waves Applicat.* **8** 329–53
[19] Erdelyi A 1956 *Asymptotic Expansions* (New York: Dover) pp 50–2
[20] Valagiannopoulos C A and Tsitsas N L 2012 Field enhancement in a grounded dielectric slab by using a single superstrate layer *Adv. Optoelectronics* **2012** 439147
[21] Valagiannopoulos C A and Tsitsas N L 2012 Integral equation analysis of a low-profile receiving planar microstrip antenna with a cloaking superstrate *Radio Sci.* **47** RS2022